ACS NANOSCIENCE Au
AN OPEN ACCESS JOURNAL OF THE AMERICAN CHEMICAL SOCIETY

pubs.acs.org/nanoau Article

Termination-Property Coupling via Reversible Oxygen Functionalization of MXenes

James L. Hart, Kanit Hantanasirisakul, Yury Gogotsi, and Mitra L. Taheri*

Cite This: *ACS Nanosci. Au* 2022, 2, 433–439 Read Online

ACCESS | Metrics & More | Article Recommendations | Supporting Information

ABSTRACT: MXenes are a growing family of 2D transition-metal carbides and nitrides, which display excellent performance in myriad of applications. Theoretical calculations suggest that manipulation of the MXene surface termination (such as =O or −F) could strongly alter their functional properties; however, experimental control of the MXene surface termination is still in the developmental stage. Here, we demonstrate that annealing MXenes in an Ar + O_2 low-power plasma results in increased =O functionalization with minimal formation of secondary phases. We apply this method to two MXenes, Ti_2CT_x and $Mo_2TiC_2T_x$ (T_x represents the mixed surface termination), and show that in both cases, the increased =O content increases the electrical resistance and decreases the surface transition-metal's electron count. For $Mo_2TiC_2O_x$, we show that the O content can be reversibly altered through successive vacuum and plasma annealing. This work provides an effective way to tune MXene surface functionalization, which may unlock exciting surface-dependent properties.

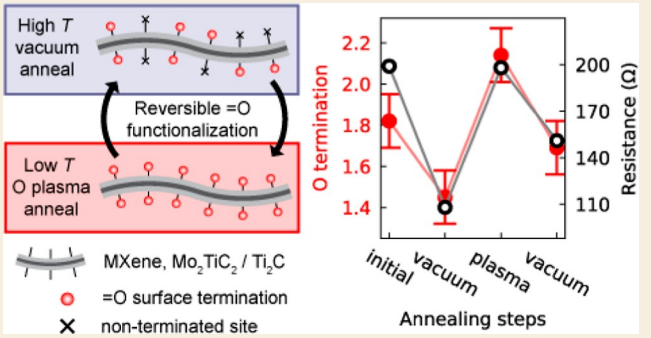

KEYWORDS: *MXenes, 2D materials, surface functionalization, electron energy loss spectroscopy, oxidation state analysis, electrical resistance measurements*

MXenes are a quickly expanding family of 2D materials that show exceptional promise for applications ranging from electromagnetic interference shielding to energy storage, gas sensing, flexible electronics, and medicine.[1−8] The MXene general formula is $M_{n+1}X_n$, where M represents one or more transition-metal element(s), X is C and/or N, and n = 1−4. So far, over 30 stoichiometric MXenes have been experimentally synthesized. In contrast to other 2D materials such as graphene or transition-metal dichalcogenides, bare MXene surfaces are composed of transition-metal layers, which are reactive and readily form chemical bonds with available terminating moieties. In fact, the MXene surfaces are invariably functionalized during synthesis, usually with a non-uniform mixture of −OH, −F, −Cl, and =O.[9−12] Thus, the MXene chemical formula is usually expanded to $M_{n+1}X_nT_x$, where T represents the mixed surface termination.

Tuning MXene functional properties *via* surface termination holds great promise, though this goal has yet to be fully experimentally realized. Numerous density functional theory (DFT) calculations have predicted that termination can strongly influence MXene properties such as Li ion capacity and mechanical strength, and in certain MXenes, altering the termination is predicted to drive metal-to-insulator transitions (MITs).[6,13−16] However, the metastable nature of MXenes and the relatively strong M−T bonds make it difficult to alter the as-synthesized mixed surface termination without degrading the underlying MXene structure. One approach to solve this problem is the development of novel synthesis methods.[17−21] Notably, the use of molten salt reactions shows great promise for the precise control of a wide range of surface groups.[19,20] A second route is post-synthesis treatment, such as vacuum annealing[10,22,23] or controlled exposure to chemical reagents.[24,25] For example, Persson et al. recently reported on the annealing of individual $Ti_3C_2T_x$ flakes in a low-pressure O_2 environment and obtained full =O functionalization,[26] though TiO_2 was formed as a secondary phase.[26,27] Despite these successes, methods to reliably and reversibly alter the MXene termination require further development. Moreover, there are only a few available reports which correlate the MXene surface termination with physical and chemical properties.

Here, we report a plasma annealing method for =O surface functionalization, which shows promise for reversible termination control in MXene thin films, with minimal secondary oxide formation (Figure 1a). Specifically, we iteratively performed vacuum annealing to drive surface defunctionalization, followed by Ar + O_2 plasma annealing to refunctionalize

Received: May 19, 2022
Revised: June 8, 2022
Accepted: June 9, 2022
Published: June 28, 2022

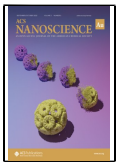

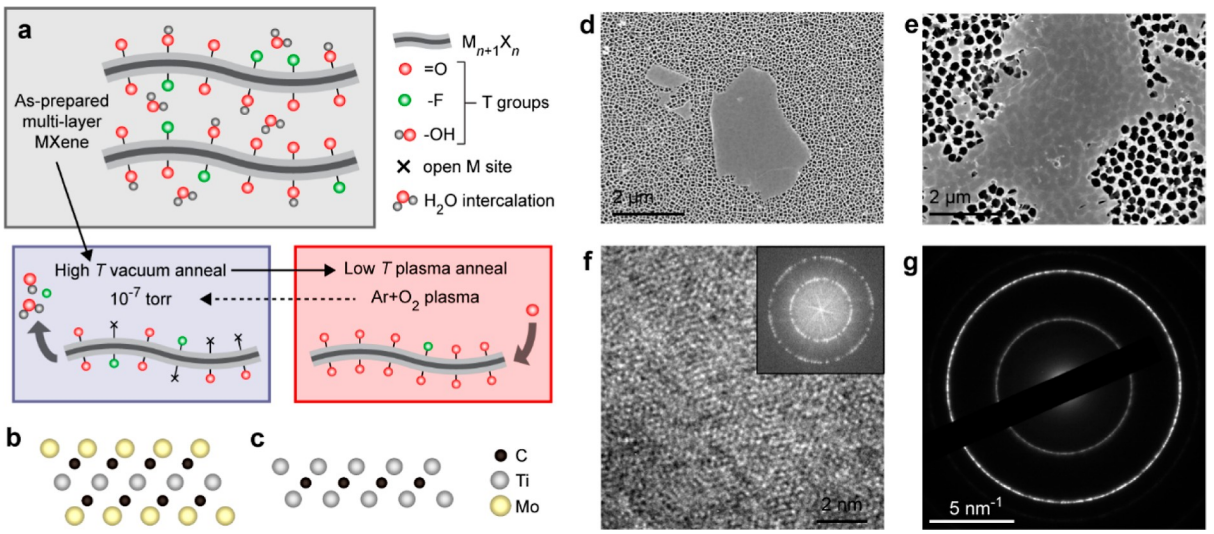

Figure 1. (a) Schematic of the experimental approach. High-temperature vacuum annealing is used to drive surface defunctionalization, and then, low-temperature annealing in an Ar + O_2 plasma is used to refunctionalize the MXene surfaces with O. (b,c) Schematics of Mo_2TiC_2 and Ti_2C, respectively. Note that the terminations are not shown. (d,e) Scanning electron microscopy images of $Mo_2TiC_2T_x$ and Ti_2CT_x flakes on anodic aluminum oxide, respectively. (f) HRTEM image of a $Mo_2TiC_2T_x$ film. The inset shows the Fourier transform of the HRTEM image. (g) Selected area electron diffraction pattern of a $Mo_2TiC_2T_x$ film.

the MXene surface and increase the relative =O concentration. Importantly, the effects of varying =O content on the MXene structure, chemistry, and electronic properties were monitored in situ using electron diffraction, electron spectroscopy, and resistance versus temperature (R vs T) measurements, respectively. We apply this technique to two MXenes, $Mo_2TiC_2T_x$ and Ti_2CT_x (Figure 1b,c), both of which show metallic conductivity in their as-synthesized, mixed-termination state but are predicted to undergo a MIT upon complete =O functionalization.[28,29] For both MXenes, our plasma annealing method leads to increased =O termination, a concomitant decrease in the surface metal's d orbital occupancy, and an increase in the electrical resistance. However, neither MXene displayed an =O induced MIT, which motivates further theoretical efforts. For $Mo_2TiC_2T_x$, we show that =O can be reversibly added and removed from the MXene surface, and we demonstrate uniform =O functionalization. Conversely, for Ti_2CT_x, reversible control of =O termination was not achieved, reflecting the differences in strength, thermal stability, and M−T bond energy between these two MXenes.[10,22,30]

Details of the bulk Mo_2TiAlC_2 and Ti_2AlC MAX phase synthesis are given in the Supporting Information. From the parent MAX phases, aqueous solutions of single-flake MXenes were synthesized according to ref 31; further details are given in the Supporting Information. Scanning electron microscopy images of individual $Mo_2TiC_2T_x$ and Ti_2CT_x MXene flakes are shown in Figure 1d,e, respectively. To enable our annealing experiments, we spin-coated MXene films onto transmission electron microscopy (TEM) chips that allow in situ annealing and biasing within TEM (Supporting Information, Figure 1).[32] The spin-coated MXene films were spatially uniform, consisting of many restacked, overlapping c-axis-oriented flakes, with thicknesses in the range of 10−50 nm. This structure is evidenced in the high-resolution TEM (HRTEM) image, as shown in Figure 1f. No individual atomic columns are observed, but clear rings are revealed in the image Fourier transform, indicative of many overlapping c-axis-oriented flakes with random in-plane rotations. The electron diffraction pattern in Figure 1g confirms this interpretation, showing strong rings corresponding to the MXene (010) and (110) reflections, as expected for our sample geometry. Given the synthesis treatments used here, the as-deposited Ti_2CT_x has initial =O, −OH, and −F termination and Li^+ and H_2O intercalation, and no secondary phases or contaminants are observed. The as-deposited $Mo_2TiC_2T_x$ has =O and −OH termination and H_2O and tetramethylammonium cation (TMA^+) intercalation. There are also trace amounts (≤1 at %) of calcium oxide contaminants in our $Mo_2TiC_2T_x$ samples, as determined from electron energy loss spectroscopy (EELS) elemental analysis and electron diffraction (Supporting Information, Figure 2). We note here that multiple Ti_2CT_x and $Mo_2TiC_2T_x$ samples were tested and showed qualitatively similar behavior (see Supporting Information, Figures 3−6).

Our experimental approach is schematically outlined in Figure 1a. With the end goal of obtaining homogeneous =O functionalization, it is first necessary to remove intercalation species and other termination moieties. Because =O termination is more stable than −OH or −F, vacuum annealing can be used to (partially) remove the non =O termination and intercalants.[10,22,23] To this end, samples were initially annealed at high temperature (400−800 °C) under the vacuum of TEM (~10^{-7} torr). Then, to (re)functionalize the exposed M-sites with =O, we removed the sample holder from the transmission electron microscope and inserted it into a plasma chamber. Samples were annealed from 100−300 °C in an Ar + O_2 plasma (80% Ar and 20% O_2) at ~1 mbar and 18 W. During sample transfer to and from the plasma chamber, the samples were exposed to the ambient atmosphere for ~10 s; however, we find that this brief exposure does not alter the oxygen content of our MXene films (Supporting Information, Figure 7). After each annealing step, EELS and electron diffraction patterns were collected from the same location of each sample to determine the composition and structure. EELS and diffraction data collected after in situ TEM vacuum annealing are labeled as V_temp, where "temp" is the vacuum

https://doi.org/10.1021/acsnanoscienceau.2c00024
ACS Nanosci. Au 2022, 2, 433−439

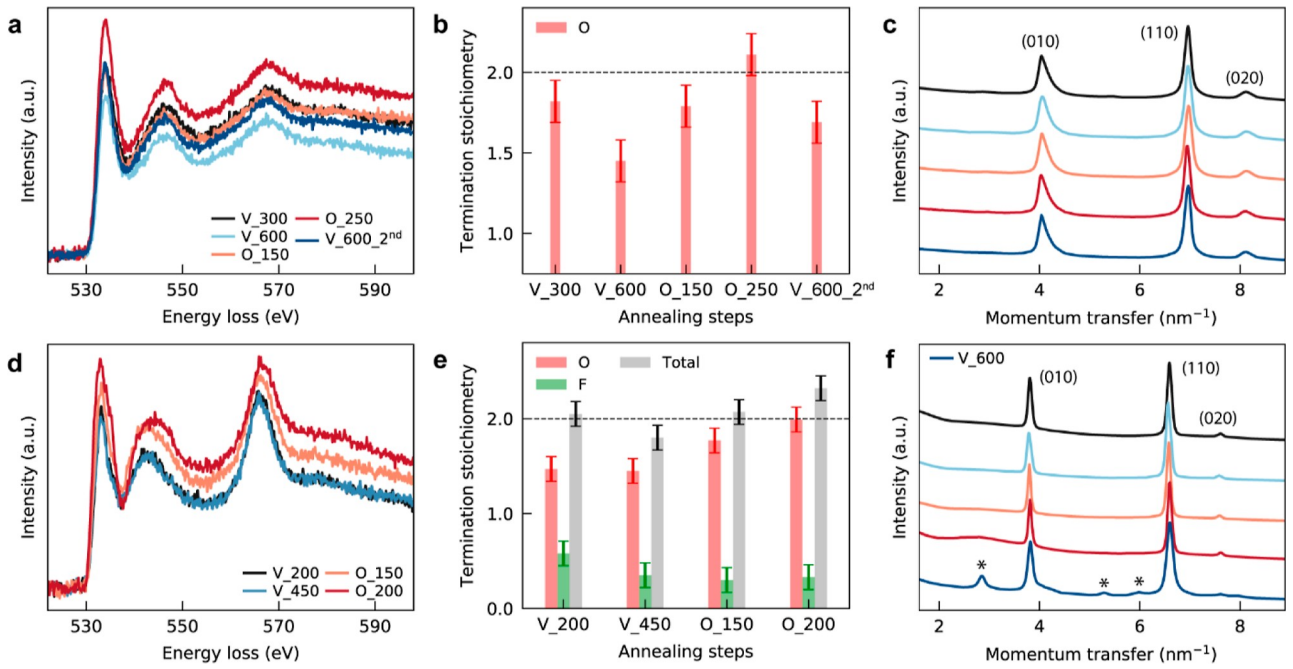

Figure 2. (a) O *K*-edge of $Mo_2TiC_2T_x$ after various annealing steps. The edge intensity was normalized based on the Ti *L*-edge intensity, see Supporting Information Figure 3. (b) Termination composition of the same $Mo_2TiC_2T_x$ sample, as determined from the EELS data. (c) RAED of $Mo_2TiC_2T_x$ after various annealing treatments. The legend in (a) applies to (c) as well. (d–f) Same as (a–c) but for a Ti_2CT_x sample. In (f), * marks anatase Ti oxide peaks. The 2D electron diffraction patterns used and the generated RAED profiles are given in Supporting Information (Figure 10).

annealing temperature in °C, and these measurements are shown with blue curves. Measurements after Ar + O_2 plasma treatments are labeled as O_temp and are shown with red curves. We used heating and cooling rates of 1 °C/s. For vacuum annealing steps, the maximum temperature was held for 5 min, and for plasma annealing steps, the maximum temperature was held for 1 min.

Our ability to alter the surface termination in $Mo_2TiC_2T_x$ is summarized in Figure 2a–c. For this sample, we used the following annealing sequence: V_300 → V_600 → O_150 → O_250 → V_600_2nd. Figure 2a shows the EELS O K-edge measured after each annealing step, and the changes in edge height are directly proportional to changes in the oxygen concentration. Figure 2b quantifies the EELS data and plots changes in the termination concentration. Lastly, Figure 2c shows the electron diffraction data. Owing to the rotational symmetry of the diffraction patterns (Figure 1g), we perform a rotational average on the raw 2D diffraction data and present the rotationally averaged electron diffraction (RAED) data, as intensity versus momentum transfer (Q). The initial 300 °C annealing step was used to drive H_2O deintercalation, which could otherwise complicate O *K*-edge EELS analysis and O concentration determination. The following 600 °C vacuum anneal, aimed at removing −OH and =O termination, resulted in a significant decrease in the O *K*-edge intensity. Presumably, the measured decrease in the O *K*-edge intensity has contributions from the loss of both −OH and =O species; however, we cannot differentiate these two moieties with EELS. Regardless, after the 600 °C annealing step, we conclude that only =O remains since −OH desorbs at temperatures well below 600 °C.[22] Following the 600 °C vacuum anneal, plasma annealing at 150 °C led to a substantial increase in the =O concentration, and subsequent plasma annealing at 250 °C produced fully functionalized $Mo_2TiC_2O_{2.1}$ (for all given MXene composition $M_{n+1}X_nT_x$, the error in x is ±0.1). To demonstrate the reversibility of this process, we then performed a second vacuum annealing step at 600 °C, which reduced the =O concentration to $Mo_2TiC_2O_{1.7}$. Note that the RAED data show no emergence of secondary phases throughout the entire experiment (Figure 2c), confirming the integrity of the MXene structure. We also note that while the O *K*-edge intensity changed substantially (which reflects changes in the oxygen content), changes to the fine structure of the O *K*-edge were negligible (Figure 2a and Supporting Information, Figure 8). The O *K*-edge fine structure reflects the bonding environment of oxygen; thus, the constant fine structure indicates that oxygen was added (and removed) from the sample in the form of =O termination, as opposed to incorporation into secondary oxides. Similarly, the C *K*- and Ti *L*-edges show negligible fine structure changes with annealing, further verifying retention of the MXene structure throughout all the annealing steps (Supporting Information, Figure 9). These data represent reversible surface termination control in $Mo_2TiC_2O_x$.

For Ti_2CT_x, the goal of obtaining uniform =O termination is impeded by three factors: initial −F termination which must be removed, lower thermal stability of Ti_2CT_x compared to $Mo_2TiC_2T_x$, and stronger Ti−T bonding relative to Mo−T bonding.[10,22,30] Consequently, attempts to completely remove −F with high-temperature vacuum annealing consistently failed; secondary oxides formed prior to complete −F removal. Thus, with the aim of minimizing −F while avoiding secondary phase formation, we used the following annealing sequence: V_200 → V_450 → O_150 → O_200. The EELS and RAED data are shown in Figure 2d–f. The initial 200 °C vacuum anneal was intended to remove H_2O intercalation, and the following 450 °C vacuum anneal resulted in a slight reduction in the −F concentration. Subsequent plasma annealing at 150

https://doi.org/10.1021/acsnanoscienceau.2c00024
ACS Nanosci. Au 2022, 2, 433–439

°C increased the =O content, giving a composition of $Ti_2CO_{1.8}F_{0.3}$ with fully saturated Ti surface sites. We note that for these annealing steps (V_200, V_450, and O_150), the RAED shows no evidence of secondary phase formation, and the O *K*-edge only changes in magnitude, with the fine structure remaining constant. These findings indicate that only the surface termination concentration is altered, while the underlying Ti_2C structure remains intact. An additional plasma anneal at 200 °C further increased the O content, resulting in a composition of $Ti_2CO_{2.0}F_{0.3}$ and suggesting super saturation of the MXene surface.[26] However, a broad peak in the RAED data at $Q \sim 3$ nm^{-1} suggests some degree of MXene degradation during the O_200 anneal, and the excess O could be contained within amorphous secondary phases. Final vacuum annealing at 600 °C did not result in any =O loss, but a measurable fraction of TiO_2 was formed, as evidenced by the TiO_2 peaks seen in the RAED data (Figure 2f). In contrast to $Mo_2TiC_2T_x$, the inability to reversibly control =O in Ti_2CT_x reflects the known differences in thermal stability and M−T bond strength of these two MXenes.[10,22,30]

Having altered the =O concentration in both $Mo_2TiC_2T_x$ and Ti_2CT_x, we next consider how changes in T influence the surface M-site chemistry. This is a critical question for understanding termination-property coupling as oxidation state changes in transition metal compounds are often associated with changes in magnetism, MITs, and other functional properties.[33] For our Mo *L*-edge EELS analysis of $Mo_2TiC_2T_x$, we investigated a separate sample than that shown in Figure 2. The $Mo_2TiC_2T_x$ sample investigated with Mo *L*-edge EELS (as shown in Figure 3a) had an annealing sequence of V_200 → V_700, and the measured post-anneal compositions were $Mo_2TiC_2O_{2.1}$ → $Mo_2TiC_2O_{1.5}$ (Supporting Information, Figure 3). With vacuum annealing and decreased =O concentration, the measured Mo L_3- and L_2-edge intensities decreased substantially. Within the experimental energy resolution and signal-to-noise ratio, no discernible changes in the Mo $L_{3,2}$-edge shapes were observed. For Ti_2CT_x, the Ti *L*-edge spectra (and their evolution with annealing) are shown in Figure 3b. We note that the initial state Ti *L*-edge data (V_200) are consistent with recent X-ray absorption spectroscopy measurements of this MXene.[31] With plasma annealing and increased =O termination, the intensity of both the Ti L_3- and L_2-edges increases, and the edge shape also evolves.

To quantify the EELS fine structure changes, we analyzed the data using the white-line intensity method. This method is based on the fact that the intensity of transition-metal *L*-edges is (to the first order) proportional to number of unoccupied transition-metal *d* orbitals, which is proportional to the oxidation state of the transition-metal ion. Thus, increasing the oxidation state of a transition-metal ion tends to increase the density of unoccupied *d* states, which increases the intensity of the EELS *L*-edge.[34] Table 1 shows the integrated $L_3 + L_2$ edge intensity for $Mo_2TiC_2T_x$ and Ti_2CT_x (see Supporting Information, Figures 11 and 12 for data processing steps). This analysis shows that an increase (decrease) in =O termination increases (decreases) the number of unoccupied M-site *d* orbitals, indicating a decrease (increase) in the M-site electron count. These data provide direct experimental evidence that =O termination alters the MXene M-site chemistry. Note that we also analyzed our data using the white-line ratio method (related to the branching ratio method);[35]

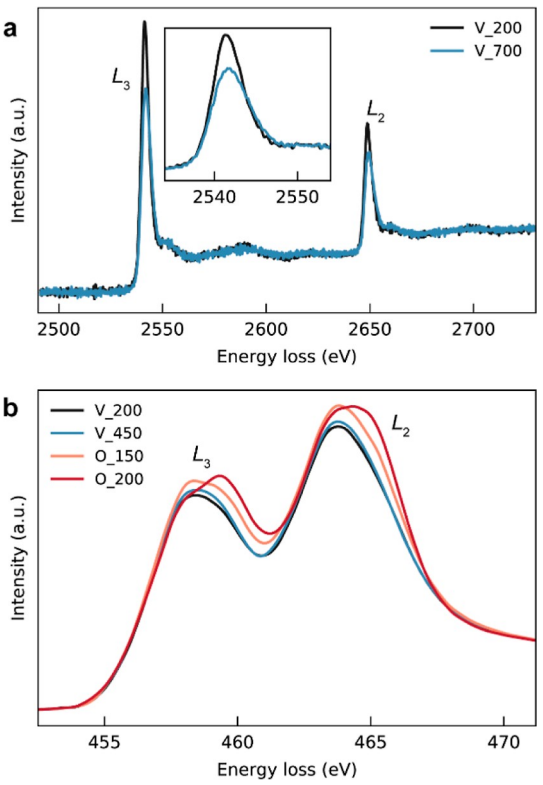

Figure 3. (a) Mo $L_{3,2}$-edges of $Mo_2TiC_2T_x$ after vacuum annealing. (b) Ti $L_{3,2}$-edges of Ti_2CT_x after various annealing steps. Due to the energy drift of the TEM, all edges were aligned to their edge onset. All spectra were deconvolved to remove plural scattering. The Ti *L*-edges were normalized to the post-edge continuum intensity (at 472 eV), and the Mo *L*-edge data were normalized to the post-L_3-edge intensity, from 2560 to 2640 eV.

Table 1. Comparison of EELS Fine Structure Analysis for $Mo_2TiC_2T_x$ and Ti_2CT_x MXenes[a,b,c]

	$Mo_2TiC_2T_x$		Ti_2CT_x			
	V_200	V_700	V_200	V_450	O_150	O_200*
O_x	2.1	1.5	1.5	1.5	1.8	2.0
$L_3 + L_2$	1.00	0.85	1.00	1.01	1.11	1.19
L_3/L_2	0.54	0.54	0.43	0.43	0.44	0.44

[a]The O_x row indicates the value of *x* in $Mo_2TiC_2O_x$ and $Ti_2CF_yO_x$. [b]For the $L_3 + L_2$ row, the values were normalized to the initial measurement. [c]The * marking the Ti_2CT_x O_200 column indicates that some MXene degradation and oxide formation may be present.

however, differences in the L_3/L_2 intensity ratio were within the analysis uncertainty and showed no strong trend (Table 1).

Lastly, we consider how changes in the =O content and *d* orbital occupancy correlate with the electronic transport properties of Ti_2CT_x and $Mo_2TiC_2T_x$. After each annealing step, we measured the resistance of the sample as a function of temperature (*R* vs *T*) upon cooling from 200 °C (Figure 4a,b). Note that the $Mo_2TiC_2T_x$ *R vs T* data presented here comes from the same sample as described in Figure 2. To understand changes in *R vs T* in the context of surface chemistry, we plot the room-temperature resistance (R_{RT}), the temperature dependence of resistance (d*R*/d*T*) at room temperature, and the =O termination content as a function of annealing conditions (Figure 4c,d). Somewhat surprisingly, Ti_2CT_x and $Mo_2TiC_2T_x$ displayed metallic conductivity (positive d*R*/d*T*)

https://doi.org/10.1021/acsnanoscienceau.2c00024
ACS Nanosci. Au 2022, 2, 433−439

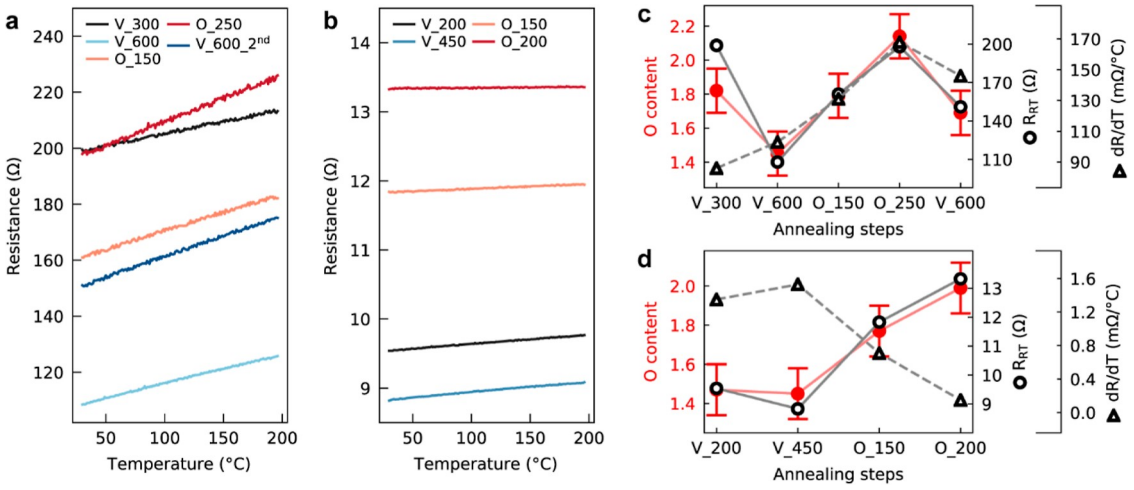

Figure 4. (a,b) R vs T results for $Mo_2TiC_2T_x$ and Ti_2CT_x, respectively. (c,d) Analysis of the R vs T data for $Mo_2TiC_2T_x$ and Ti_2CT_x, respectively. Lines are a guide for the eye.

for all annealing conditions; we did not observe a MIT in either $Ti_2CO_{2.0}F_{0.3}$ or $Mo_2TiC_2O_{2.1}$. For Ti_2CT_x, the absence of a MIT with increased =O functionalization may be due to the residual −F content since Ti_2CF_2 is predicted to be a metal.[36] Importantly, $Ti_2CO_{2.0}F_{0.3}$ showed an almost temperature-independent resistance in the entire range under study. This behavior is very important for electronic applications as it provides stable performance even upon large temperature fluctuations. For $Mo_2TiC_2O_{2.1}$, the absence of semiconducting behavior may be related to extrinsic effects, for example, point defects or disorder of the Ti and Mo sublattices. Alternatively, the measured metallic conductivity may be an intrinsic property of $Mo_2TiC_2O_2$, as predicted in certain DFT studies.[37,38]

Despite the absence of a MIT, interesting trends still emerge from the data presented in Figure 4. For both $Mo_2TiC_2T_x$ and Ti_2CT_x, there is a clear correlation between =O content and R_{RT}. In a previous study, we found a similar correlation between −F content and R_{RT} in $Ti_3C_2T_x$ and Ti_3CNT_x.[22] For $Ti_3C_2T_x$ and Ti_3CNT_x, an increased −F content also led to an increase in dR/dT. Conversely, in the present study, the increasing =O content caused a decrease in dR/dT for Ti_2CT_x, suggesting a different mechanism linking the surface termination and electrical resistance. However, we note the challenges associated with analysis of multi-flake MXene R *vs* T measurements, which include contributions from both inter-flake and intra-flake effects.[22,39]

In conclusion, we used a low power Ar + O_2 plasma annealing method to tune the =O functionalization in both $Mo_2TiC_2T_x$ and Ti_2CT_x films. For $Mo_2TiC_2T_x$, we obtained pure =O functionalization and were able to reversibly add and remove =O from the MXene surface. For both MXenes, increased =O functionalization leads to a decrease in the surface M-site d orbital occupancy. This finding offers important insights into how surface termination alters the MXene chemistry with direct relevance for applications such as catalysis. From R *vs* T measurements, we found that increasing =O termination increased the MXene electrical resistance. Despite predicted MITs in both MXenes, we found that $Mo_2TiC_2O_{2.1}$ and $Ti_2CO_{2.0}F_{0.3}$ are metallic, which motivates further theoretical investigation into the electronic structures of these materials. Notably, Ti_2CT_x approached temperature-independent resistance when the =O termination was maximized, which is important for certain electronic applications. At present, the microscopic mechanism of MXene functionalization during plasma annealing is not known, and additional work is needed in this direction. The plasma annealing method described here holds promise for control of MXene surface functionalization, which, in turn, allows tailoring of the MXene resistance and chemistry for application-specific property optimization.

■ ASSOCIATED CONTENT

Supporting Information

The Supporting Information is available free of charge at https://pubs.acs.org/doi/10.1021/acsnanoscienceau.2c00024.

Materials and methods; additional EELS and diffraction results; and data on additional Ti_2CT_x and $Mo_2TiC_2T_x$ samples (PDF)

■ AUTHOR INFORMATION

Corresponding Author

Mitra L. Taheri − *Department of Materials Science and Engineering, Johns Hopkins University, Baltimore, Maryland 21218, United States;* orcid.org/0000-0001-5349-1411; Email: mtaheri4@jhu.edu

Authors

James L. Hart − *Department of Materials Science and Engineering, Johns Hopkins University, Baltimore, Maryland 21218, United States; Department of Materials Science and Engineering, Drexel University, Philadelphia, Pennsylvania 19104, United States;* Present Address: Department of Mechanical Engineering and Materials Science, Yale University, New Haven, CT 06511, USA; orcid.org/0000-0002-2960-6925

Kanit Hantanasirisakul − *Department of Materials Science and Engineering and A. J. Drexel Nanomaterials Institute, Drexel University, Philadelphia, Pennsylvania 19104, United States;* orcid.org/0000-0002-4890-1444

Yury Gogotsi − *Department of Materials Science and Engineering and A. J. Drexel Nanomaterials Institute, Drexel University, Philadelphia, Pennsylvania 19104, United States;* orcid.org/0000-0001-9423-4032

https://doi.org/10.1021/acsnanoscienceau.2c00024
ACS Nanosci. Au 2022, 2, 433−439

Complete contact information is available at:
https://pubs.acs.org/10.1021/acsnanoscienceau.2c00024

Author Contributions

The manuscript was written through contributions of all authors. All authors have given approval to the final version of the manuscript.

Notes

The authors declare no competing financial interest.

■ ACKNOWLEDGMENTS

J.L.H. and M.L.T. acknowledge funding in part from the National Science Foundation (NSF) MRI Award #DMR-1429661 and in part from the U.S. Department of Energy, Office of Basic Energy Sciences through contract DE-SC0020314.. The work on MXene synthesis at the Drexel University was funded by the U.S. Department of Energy (DOE), Office of Science, Office of Basic Energy Sciences, grant #DESC0018618. Mark Anayee (Drexel University) is acknowledged for providing XRD data of the Mo_2TiAlC_2 MAX phase.

■ REFERENCES

(1) Naguib, M.; Kurtoglu, M.; Presser, V.; Lu, J.; Niu, J.; Heon, M.; Hultman, L.; Gogotsi, Y.; Barsoum, M. W. Two-Dimensional Nanocrystals Produced by Exfoliation of Ti_3AlC_2. *Adv. Mater.* **2011**, *23*, 4248−4253.
(2) Verger, L.; Natu, V.; Carey, M.; Barsoum, M. W. MXenes: An Introduction of Their Synthesis, Select Properties, and Applications. *Trends Chem.* **2019**, *1*, 656−669.
(3) Shahzad, F.; Alhabeb, M.; Hatter, C. B.; Anasori, B.; Man Hong, S.; Koo, C. M.; Gogotsi, Y. Electromagnetic Interference Shielding with 2D Transition Metal Carbides (MXenes). *Science* **2016**, *353*, 1137−1140.
(4) Sarycheva, A.; Polemi, A.; Liu, Y.; Dandekar, K.; Anasori, B.; Gogotsi, Y. 2D Titanium Carbide (MXene) for Wireless Communication. *Sci. Adv.* **2018**, *4*, No. eaau0920.
(5) Chaudhari, N. K.; Jin, H.; Kim, B.; San Baek, D.; Joo, S. H.; Lee, K. MXene: An Emerging Two-Dimensional Material for Future Energy Conversion and Storage Applications. *J. Mater. Chem. A* **2017**, *5*, 24564−24579.
(6) Hantanasirisakul, K.; Gogotsi, Y. Electronic and Optical Properties of 2D Transition Metal Carbides and Nitrides (MXenes). *Adv. Mater.* **2018**, *30*, 1804779.
(7) Khazaei, M.; Ranjbar, A.; Arai, M.; Sasaki, T.; Yunoki, S. Electronic Properties and Applications of MXenes: A Theoretical Review. *J. Mater. Chem. C* **2017**, *5*, 2488−2503.
(8) Zhu, J.; Ha, E.; Zhao, G.; Zhou, Y.; Huang, D.; Yue, G.; Hu, L.; Sun, N.; Wang, Y.; Lee, L. Y. S.; Xu, C.; Wong, K.-Y.; Astruc, D.; Zhao, P. Recent Advance in MXenes: A Promising 2D Material for Catalysis, Sensor and Chemical Adsorption. *Coord. Chem. Rev.* **2017**, *352*, 306−327.
(9) Hope, M. A.; Forse, A. C.; Griffith, K. J.; Lukatskaya, M. R.; Ghidiu, M.; Gogotsi, Y.; Grey, C. P. NMR Reveals the Surface Functionalisation of Ti_3C_2. *Phys. Chem. Chem. Phys.* **2016**, *18*, 5099−5102.
(10) Persson, I.; Naslund, L.-A.; Halim, J.; Barsoum, M. W.; Darakchieva, V.; Palisaitis, J.; Rosen, J.; Persson, P. O. A. On the Organization and Thermal Behavior of Functional Groups on Ti_3C_2 MXene Surfaces in Vacuum. *2D Mater.* **2018**, *5*, 015002.
(11) Wang, H.-W.; Naguib, M.; Page, K.; Wesolowski, D. J.; Gogotsi, Y. Resolving the Structure of $Ti_3C_2T_x$ MXenes through Multilevel Structural Modeling of the Atomic Pair Distribution Function. *Chem. Mater.* **2016**, *28*, 349−359.
(12) Magne, D.; Mauchamp, V.; Célérier, S.; Chartier, P.; Cabioc'h, T. Site-Projected Electronic Structure of Two-Dimensional Ti_3C_2 MXene: The Role of the Surface Functionalization Groups. *Phys. Chem. Chem. Phys.* **2016**, *18*, 30946.
(13) Dong, L.; Kumar, H.; Anasori, B.; Gogotsi, Y.; Shenoy, V. B. Rational Design of Two-Dimensional Metallic and Semiconducting Spintronic Materials Based on Ordered Double-Transition-Metal MXenes. *J. Phys. Chem. Lett.* **2017**, *8*, 422−428.
(14) Bai, Y.; Zhou, K.; Srikanth, N.; Pang, J. H. L.; He, X.; Wang, R. Dependence of Elastic and Optical Properties on Surface Terminated Groups in Two-Dimensional MXene Monolayers: A First-Principles Study. *RSC Adv.* **2016**, *6*, 35731−35739.
(15) Lee, Y.; Hwang, Y.; Chung, Y.-C. Achieving Type i, ii, and iii Heterojunctions Using Functionalized MXene. *ACS Appl. Mater. Interfaces* **2015**, *7*, 7163−7169.
(16) Xie, Y.; Naguib, M.; Mochalin, V. N.; Barsoum, M. W.; Gogotsi, Y.; Yu, X.; Nam, K.-W.; Yang, X.-Q.; Kolesnikov, A. I.; Kent, P. R. C. Role of Surface Structure on Li-Ion Energy Storage Capacity of Two-Dimensional Transition-Metal Carbides. *J. Am. Chem. Soc.* **2014**, *136*, 6385−6394.
(17) Natu, V.; Pai, R.; Sokol, M.; Carey, M.; Kalra, V.; Barsoum, M. W. 2D $Ti_3C_2T_z$ MXene Synthesized by Water-Free Etching of Ti_3AlC_2 in Polar Organic Solvents. *Chem* **2020**, *6*, 616−630.
(18) Yang, S.; Zhang, P.; Wang, F.; Ricciardulli, A. G.; Lohe, M. R.; Blom, P. W. M.; Feng, X. Fluoride-Free Synthesis of Two-Dimensional Titanium Carbide (MXene) Using A Binary Aqueous System. *Angew. Chem.* **2018**, *130*, 15717−15721.
(19) Li, M.; Lu, J.; Luo, K.; Li, Y.; Chang, K.; Chen, K.; Zhou, J.; Rosen, J.; Hultman, L.; Eklund, P.; Persson, P. O. Å.; Du, S.; Chai, Z.; Huang, Z.; Huang, Q. Element Replacement Approach by Reaction with Lewis Acidic Molten Salts to Synthesize Nanolaminated MAX Phases and MXenes. *J. Am. Chem. Soc.* **2019**, *141*, 4730−4737.
(20) Kamysbayev, V.; Filatov, A.; Hu, H.; Rui, X.; Lagunas, F.; Wang, D.; Klie, R.; Talapin, D. Covalent Surface Modifications and Superconductivity of Two-Dimensional Metal Carbide MXenes. *Science* **2020**, *8311*, No. eaba8311.
(21) Lu, J.; Persson, I.; Lind, H.; Palisaitis, J.; Li, M.; Li, Y.; Chen, K.; Zhou, J.; Du, S.; Chai, Z.; Huang, Z.; Hultman, L.; Eklund, P.; Rosen, J.; Huang, Q.; Persson, P. O. Å. $Ti_{n+1}C_n$ MXenes with Fully Saturated and Thermally Stable Cl Terminations. *Nanoscale Adv.* **2019**, *1*, 3680−3685.
(22) Hart, J. L.; Hantanasirisakul, K.; Lang, A. C.; Anasori, B.; Pinto, D.; Pivak, Y.; van Omme, J. T.; May, S. J.; Gogotsi, Y.; Taheri, M. L. Control of MXenes' Electronic Properties through Termination and Intercalation. *Nat. Commun.* **2019**, *10*, 522.
(23) Hart, J. L.; Hantanasirisakul, K.; Lang, A. C.; Li, Y.; Mehmood, F.; Pachter, R.; Frenkel, A. I.; Gogotsi, Y.; Taheri, M. L. Multimodal Spectroscopic Study of Surface Termination Evolution in $Cr_2TiC_2T_x$ MXene. *Adv. Mater. Interfaces* **2021**, *8*, 2001789.
(24) Persson, I.; Halim, J.; Lind, H.; Hansen, T. W.; Wagner, J. B.; Näslund, L. Å.; Darakchieva, V.; Palisaitis, J.; Rosen, J.; Persson, P. O. Å. 2D Transition Metal Carbides (MXenes) for Carbon Capture. *Adv. Mater.* **2019**, *31*, No. e1805472.
(25) Halim, J.; Persson, I.; Eklund, P.; Persson, P. O. Å.; Rosen, J. Sodium Hydroxide and Vacuum Annealing Modifications of the Surface Terminations of a Ti_3C_2 (MXene) Epitaxial Thin Film. *RSC Adv.* **2018**, *8*, 36785−36790.
(26) Persson, I.; Halim, J.; Hansen, T. W.; Wagner, J. B.; Darakchieva, V.; Palisaitis, J.; Rosen, J.; Persson, P. O. Å. How Much Oxygen Can a MXene Surface Take Before It Breaks? *Adv. Funct. Mater.* **2020**, *30*, 1909005.
(27) Ghassemi, H.; Harlow, W.; Mashtalir, O.; Beidaghi, M.; Lukatskaya, M. R.; Gogotsi, Y.; Taheri, M. L. In Situ Environmental Transmission Electron Microscopy Study of Oxidation of Two-Dimensional Ti_3C_2 and Formation of Carbond-Supported TiO_2. *J. Mater. Chem. C* **2014**, *2*, 14339−14343.
(28) Xie, Y.; Kent, P. R. C. Hybrid Density Functional Study of Structural and Electronic Properties of Functionalized $Ti_{n+1}X_n$ (X=C,N) Monolayers. *Phys. Rev. B: Condens. Matter Mater. Phys.* **2013**, *87*, 235441.

(29) Khazaei, M.; Ranjbar, A.; Arai, M.; Yunoki, S. Topological Insulators in Ordered Double Transition Metals M'_2MC_2 (M=Mo, W; M=Ti, Zr, Hf) MXenes. *Phys. Rev. B* **2016**, *94*, 125152.
(30) Li, J.; Du, Y.; Huo, C.; Wang, S.; Cui, C. Thermal Stability of Two-Dimensional Ti_2C Nanosheets. *Ceram. Int.* **2015**, *41*, 2631−2635.
(31) Yang, Y.; Hantanasirisakul, K.; Frey, N. C.; Anasori, B.; Green, R. J.; Rogge, P. C.; Waluyo, I.; Hunt, A.; Shafer, P.; Arenholz, E.; Shenoy, V. B.; Gogotsi, Y.; May, S. J. Distinguishing Electronic Contributions of Surface and Sub-Surface Transition Metal Atoms in Ti-Based MXenes. *2D Mater.* **2020**, *7*, 025015.
(32) Pérez Garza, H. H.; Zuo, K.; Pivak, Y.; Morsink, D.; Zakhozheva, M.; Pen, M.; van Weperen, S.; Xu, Q. MEMS-Based System for In-Situ Biasing and Heating Solutions inside the TEM. *European Microscopy Congress 2016: Proceedings*; European Microscopy Congress, 2016; pp 237−238.
(33) Millis, A. J. Lattice Effects in Magnetoresistive Manganese Perovskites. *Nature* **1998**, *392*, 147−150.
(34) Pearson, D. H.; Ahn, C. C.; Fultz, B. White Lines and D-Electron Occupancies for the 3d and 4d Transition Metals. *Phys. Rev. B: Condens. Matter Mater. Phys.* **1993**, *47*, 8471.
(35) Tan, H.; Verbeeck, J.; Abakumov, A.; Van Tendeloo, G. Oxidation State and Chemical Shift Investigation in Transition Metal Oxides by EELS. *Ultramicroscopy* **2012**, *116*, 24−33.
(36) Zhang, R.-Z.; Cui, H.-L.; Li, X.-H. First-Principles Study of Structural, Electronic and Optical Properties of Doped Ti_2CF_2 MXenes. *Phys. B* **2019**, *561*, 90−96.
(37) Anasori, B.; Xie, Y.; Beidaghi, M.; Lu, J.; Hosler, B. C.; Hultman, L.; Kent, P. R. C.; Gogotsi, Y.; Barsoum, M. W. Two-Dimensional, Ordered, Double Transition Metal Carbides (MXenes). *ACS Nano* **2015**, *9*, 9507−9516.
(38) Anasori, B.; Shi, C.; Moon, E. J.; Xie, Y.; Voigt, C. A.; Kent, P. R. C.; May, S. J.; Billinge, S. J. L.; Barsoum, M. W.; Gogotsi, Y. Control of Electronic Properties of 2D Carbides (MXenes) by Manipulating Their Transition Metal Layers. *Nanoscale Horiz.* **2016**, *1*, 227−234.
(39) Halim, J.; Moon, E. J.; Eklund, P.; Rosen, J.; Barsoum, M. W.; Ouisse, T. Variable Range Hopping and Thermally Activated Transport in Molybdenum-Based MXenes. *Phys. Rev. B* **2018**, *98*, 104202.

https://doi.org/10.1021/acsnanoscienceau.2c00024
ACS Nanosci. Au 2022, 2, 433−439